Research Article Vol. 39, No. 8 / August 2022 / Journal of the Optical Society of America A 1513

Journal of the Optical Society of America A

OPTICS, IMAGE SCIENCE, AND VISION

Monte Carlo–transformed field expansion method for simulating electromagnetic wave scattering by multilayered random media

KELSEY ULMER,[1,*] JUNSHAN LIN,[1] AND DAVID P. NICHOLLS[2]

[1]Department of Mathematics and Statistics, Auburn University, Auburn, Alabama 36849, USA
[2]Department of Mathematics, Statistics, and Computer Science, University of Illinois at Chicago, Chicago, Illinois 60607, USA
*Corresponding author: kau0001@auburn.edu

Received 12 May 2022; revised 10 July 2022; accepted 10 July 2022; posted 11 July 2022; published 1 August 2022

We present an efficient numerical method for simulating the scattering of electromagnetic fields by a multilayered medium with random interfaces. The elements of this algorithm, the Monte Carlo–transformed field expansion method, are (i) an interfacial problem formulation in terms of impedance-impedance operators, (ii) simulation by a high-order perturbation of surfaces approach (the transformed field expansions method), and (iii) efficient computation of the wave field for each random sample by forward and backward substitutions. Our perturbative formulation permits us to solve a sequence of linear problems featuring an operator that is *deterministic*, and its LU decomposition matrices can be reused, leading to significant savings in computational effort. With an extensive set of numerical examples, we demonstrate not only the robust and high-order accuracy of our scheme for small to moderate interface deformations, but also how Padé summation can be used to address large deviations.

https://doi.org/10.1364/JOSAA.463346

1. INTRODUCTION

We consider the scattering of electromagnetic waves by a structure consisting of multiple layers that are separated by random interfaces that are invariant in the y direction. Figure 1 shows a representative cross section of one such structure in the x–z plane. The material in each layer is characterized by its permeability and permittivity, and we suppose incident radiation illuminates the structure from above with electric/magnetic fields that are aligned with the invariant (y) direction of the grating grooves. We are interested in efficiently finding the statistics (mean and variance) of the resulting scattered fields in each layer. The model arises from applications in physics and engineering including remote sensing [1,2], oceanography [3,4], surface plasmon resonances [5–8], and solar cells [9,10] to name just a few.

Perturbation or Kirchoff theories may be applied to random interface problems to obtain analytical solutions when the interfacial deviations are sufficiently small and smooth [11–13]. Alternatively, a numerical approach one can take is to transform the random domain into a deterministic one and to numerically approximate the transformed stochastic problem with either Monte Carlo simulations [14,15] or stochastic Galerkin methods [16,17]. Such numerical algorithms can be quite expensive as, for instance, the Monte Carlo method requires a solution of the full system of governing equations for each random sample, and the size of such systems associated to the stochastic Galerkin method becomes enormous [16,17]. For other numerical approaches to random surface problems, we refer the interested reader to [18,19].

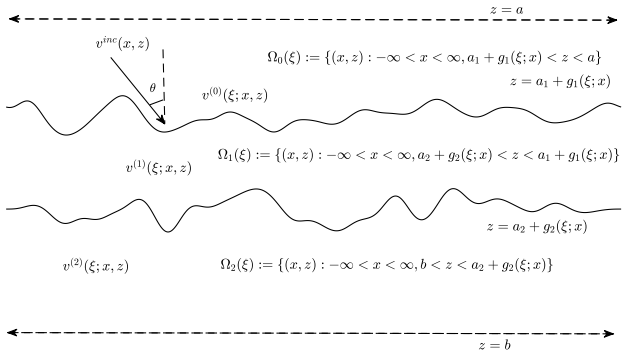

Fig. 1. Sample of a structure with three layers separated by random interfaces with artificial boundaries.

We propose an improvement of the Monte Carlo–transformed field expansion (MCTFE) method [20] to avoid the singularities generated by use of Dirichlet-to-Neumann operators on the inner layers. The components of this new MCTFE algorithm are (i) an interfacial problem formulation in terms of impedance-impedance operators (IIOs), (ii) a high-order perturbation of surfaces (HOPS) approach [the transformed field expansions (TFE) method] for solving the

model, (iii) efficient computation of the solution with forward and backward substitutions. The proposed method is a high-order spectral method and demonstrates high accuracy as is characteristic of such methods [21–23]. It requires significantly fewer unknowns compared to volumetric methods, making it far more efficient for the interfacial problems we investigate here. To make this more precise, this contribution focuses on layer interfaces of the form

$$z = a_m + g_m(x) = a_m + \varepsilon f_m(x), \quad \varepsilon \ll 1, \quad f_m = \mathcal{O}(1).$$

HOPS algorithms are particularly advantageous for such problems, as they recover the Taylor coefficients in an ε expansion of the scattered fields, which can then be summed for quite *arbitrary* values of ε (sufficiently small). Additionally, using IIOs to formulate the boundary conditions at the interfaces separating the layers avoids artificial singularities and provides a well-conditioned and stable algorithm for all wavenumbers.

Of paramount importance (see [20]), the method delivers a *deterministic* differential operator, whose inverse can be *precomputed* for use at *every* Monte Carlo sample and perturbation order. This clearly reduces the computational complexity by an enormous amount, thereby enabling, with rather modest effort, simulations that would be prohibitive for competing algorithms, e.g., classical Monte Carlo [14,15] or stochastic Galerkin [16,17], that require a full system solve for every realization. This contribution describes results found in the Ph.D. thesis of one of the authors (K. Ulmer) [24], and we refer to both [20] for a description of the MCTFE method as applied to a single random interface (which does not have inner-layer singularities), and to [25] for the development of the TFE method for simulating IIOs on domains with deterministic interfaces.

The remainder of the paper is organized as follows: Section 2 discusses the mathematical problem, while in Section 3 we present a novel surface formulation. Section 4 prescribes the numerical algorithm and its computational complexity, and Section 5 presents numerical results. Finally, Section 6 provides a brief summary of our findings.

2. MATHEMATICAL MODEL

We now provide a brief specification of the governing mathematical equations of the problem we consider.

A. Problem Formulation

Consider the scattering of electromagnetic waves by a structure consisting of multiple layers with M-many periodic random interfaces, invariant in the y direction; see Fig. 1 for one realization of such a structure. For a random sample ξ we define, for $1 \le m \le M$, the mth interface:

$$\Gamma_m(\xi) = \{(x, z): z = a_m + g_m(\xi; x)\}, \quad g_m(\xi; x + d) = g_m(\xi; x),$$

and, for $1 \le m \le M-1$, the mth layer:

$$\Omega_m(\xi) = \{(x, z): a_{m-1} + g_{m-1}(\xi; x) < z < a_m + g_m(\xi; x)\}.$$

The upper and lower layers are defined by $\Omega_0(\xi) = \{z > a_1 + g_1(\xi; x)\}$ and $\Omega_M(\xi) = \{z < a_M + g_M(\xi; x)\}$, respectively. The interface shapes are stationary Gaussian processes, and $\mathbf{n}^{(m)}$ denotes the upward pointing normal vector at interface m.

Suppose an incident plane-wave in transverse-electric (TE) or transverse-magnetic (TM) polarization illuminates the structure from above, and its transverse component is given by

$$\underline{v}^{\text{inc}}(x, z, t) = e^{i\omega t} e^{i(\alpha x - \gamma^{(0)} z)} = e^{i\omega t} v^{\text{inc}}(x, z),$$

where $\alpha = k^{(0)} \sin(\theta)$, $\gamma^{(0)} = k^{(0)} \cos(\theta)$, and θ is the angle of incidence. In each layer, given the index of refraction $n^{(m)}$, the wavenumber is given by $k^{(m)} = n^{(m)} k_0$, where $k_0 = \omega / c_0$, ω is the angular frequency of the incident wave, and c_0 is the speed of light in the vacuum. We assume that the upper and lower layers each consist of dielectrics so that $n^{(0)}, n^{(M)} \in \mathbf{R}$. While we focus upon TE polarization, TM polarization can be accommodated in an analogous fashion with a slight change in boundary conditions. Our goal is to find the statistics (mean and variance) of the scattered fields, $v^{(m)}(\xi; x, z)$, in each layer.

In TE polarization, the transverse component of the scattered electric field $v^{(m)}$ is governed by the Helmholtz equation

$$\Delta v^{(m)}(\xi; \cdot) + (k^{(m)})^2 v^{(m)}(\xi; \cdot) = 0, \quad \text{in } \Omega_m(\xi).$$

The transverse component of the total electric field and its normal derivative are both continuous, and the fields in each layer are quasiperiodic [26], i.e.,

$$v^{(m)}(\xi; x + d, z) = e^{i\alpha d} v^{(m)}(\xi; x, z), \quad 0 \le m \le M.$$

Therefore, the full set of governing equations for our model is

$$\begin{cases} \Delta v^{(m)}(\xi; \cdot) + (k^{(m)})^2 v^{(m)}(\xi; \cdot) = 0, \quad (x, z) \in \Omega_m(\xi), \quad m = 0, \dots, M, \\ v^{(0)}(\xi; \cdot) - v^{(1)}(\xi; \cdot) = -v^{\text{inc}}, \quad , z = a_1 + g_1(\xi; x), \\ \frac{\partial v^{(0)}}{\partial \mathbf{n}^{(1)}}(\xi; \cdot) - \frac{\partial v^{(1)}}{\partial \mathbf{n}^{(1)}}(\xi; \cdot) = -\frac{\partial v^{\text{inc}}}{\partial \mathbf{n}^{(1)}}, \quad z = a_1 + g_1(\xi; x), \\ v^{(m-1)}(\xi; \cdot) - v^{(m)}(\xi; \cdot) = 0, \quad z = a_m + g_m(\xi; x), \quad m = 2, \dots, M, \\ \frac{\partial v^{(m-1)}}{\partial \mathbf{n}^{(m)}}(\xi; \cdot) - \frac{\partial v^{(m)}}{\partial \mathbf{n}^{(m)}}(\xi; \cdot) = 0, \quad z = a_m + g_m(\xi; x), \quad m = 2, \dots, M, \\ v^{(m)}(\xi; x + d, z) = e^{i\alpha d} v^{(m)}(\xi; x, z), \quad m = 0, \dots, M. \end{cases} \tag{1}$$

We are only missing a description of how the fields behave at infinity, which we now presently supply.

B. Outgoing Wave Condition

The far-field behavior of waves scattered by a diffraction grating is specified by the outgoing wave condition (OWC). In this section, we make this precise for solutions in the upper layer, $\Omega_0(\xi)$, and note that a similiar analysis can be conducted in the lower. To begin, we choose $a > a_1 + |g_1|_{L^\infty}$ and define the artificial boundary $\{z = a\}$ [20,25,27] (see Fig. 1). In the domain $\{z > a\}$, the Rayleigh expansion [26,28] (for a fixed random sample ξ) expresses the scattered field in terms of the arbitrary Fourier coefficients $\hat{\psi}_p$ as

$$v^{(0)}(\xi; x, z) = \sum_{p=-\infty}^{\infty} \hat{\psi}_p e^{i\alpha_p x + i\gamma_p^{(0)}(z-a)}, \tag{2}$$

where, for $p \in \mathbb{Z}$,

$$\alpha_p := \alpha + \left(\frac{2\pi}{d}\right) p, \quad \gamma_p^{(m)} = \sqrt{(k^{(m)})^2 - \alpha_p^2}, \quad \text{Im}(\gamma_p^{(m)}) \ge 0.$$

In the case that the mth layer is a dielectric, we have

$$\gamma_p^{(m)} = \begin{cases} \sqrt{(k^{(m)})^2 - \alpha_p^2}, & p \in P^{(m)}, \\ i\sqrt{\alpha_p^2 - (k^{(m)})^2}, & p \notin P^{(m)}, \end{cases}$$

where $P^{(m)} := \{p \in \mathbb{Z} : \alpha_p^2 \leq (k^{(m)})^2\}$. This expansion defines the function $\psi(\xi; x) := v^{(0)}(\xi; x, a)$, which we utilize presently.

Enforcing continuity across the artificial boundary gives a *transparent* boundary condition in terms of a Dirichlet-to-Neumann operator (DNO). As its name suggests, this DNO maps Dirichlet data to corresponding Neumann data at the artificial boundary

$$T^{(0)} : v^{(0)}(\xi; x, a) \to \partial_z v^{(0)}(\xi; x, a).$$

From the Rayleigh expansions above, Eq. (2), we can show that

$$\partial_z v^{(0)}(\xi; x, a) = \sum_{p=-\infty}^{\infty} i\gamma_p^{(0)} \hat{\psi}_p e^{i\alpha_p x} =: T^{(0)}[\psi(\xi; x)],$$

which defines the DNO, $T^{(0)}$. With this, the OWC can be expressed as

$$\partial_z v^{(0)}(\xi; \cdot) - T^{(0)}[v^{(0)}](\xi; \cdot) = 0, \quad z = a.$$

In a similar manner, the OWC in the lower layer can be enforced with

$$\partial_z v^{(M)}(\xi; \cdot) - T^{(M)}[v^{(M)}](\xi; \cdot) = 0, \quad z = b,$$

where $T^{(M)}$ is defined in an analogous manner as $T^{(0)}$.

C. Random Surfaces: The Karhunen–Loève Expansion

We use the Karhunen–Loève expansion to represent the stationary Gaussian processes $\tilde{g}_m(\xi; x)$, $1 \leq m \leq M$, which describe the interfaces separating each layer. We assume the surface deviations are small by setting $g_m(\xi; x) = \varepsilon \tilde{g}_m(\xi; x)$, where $\varepsilon \ll 1$ and $\tilde{g}_m(\xi; x) = \mathcal{O}(1)$ are stationary Gaussian processes with continuous and bounded covariance functions. As a stationary Gaussian process, each $\tilde{g}_m(\xi; x)$ is jointly normal and has a continuous and bounded (Gaussian) covariance function

$$C^{(m)}(x, y) = c^{(m)}(x - y) = (\sigma_0^{(m)})^2 e^{-|x-y|^2/(l_c)^2},$$

where $\sigma_0^{(m)}$ is the standard deviation of the surface and l_c is the correlation length [29], each of which dictate the shape of the interface.

Since $c^{(m)}(x)$ is an even function and $\tilde{g}_m(\xi, x)$ is periodic, we may expand the covariance function in a Fourier cosine series

$$c^{(m)}(x) = \frac{\hat{c}_0^{(m)}}{2} + \sum_{p=1}^{\infty} \hat{c}_p^{(m)} \cos\left(\frac{2\pi p x}{d}\right).$$

We denote by $K^{(m)}$ the covariance operator for the mth layer:

$$K^{(m)}\phi(x) := \int_0^d c^m(x - y)\phi(y)\, \mathrm{d}y,$$

and, by direct calculation, we have that $K^{(m)}$ has eigenvalues $\lambda_j^{(m)} = d\hat{c}_j^{(m)}/2$, $j \geqslant 0$, with corresponding eigenfunctions

$$\phi_j^{(m)}(x) = \begin{cases} \sqrt{\frac{1}{d}}, & j = 0, \\ \sqrt{\frac{2}{d}} \cos\left(\frac{2j\pi x}{d}\right), & j \geqslant 2, \text{ when } j \text{ is even}, \\ \sqrt{\frac{2}{d}} \sin\left(\frac{2j\pi x}{d}\right), & j \geqslant 1, \text{ when } j \text{ is odd}. \end{cases}$$

The Karhunen–Loève expansion of $\tilde{g}_m(\xi; x)$, $1 \leq m \leq M$, is now given by

$$\begin{aligned} \tilde{g}_m(\xi; x) = \bar{g}_m(x) &+ \sqrt{\lambda_0^{(m)}}\sqrt{\frac{1}{d}}\zeta_0^{(m)}(\xi) \\ &+ \sum_{j=1}^{\infty} \sqrt{\lambda_j^{(m)}}\sqrt{\frac{2}{d}} \left[\zeta_{2j}^{(m)}(\xi) \cos\left(\frac{2(2j)\pi x}{d}\right)\right. \\ &\left. + \zeta_{2j-1}^{(m)}(\xi) \sin\left(\frac{2(2j-1)\pi x}{d}\right)\right], \end{aligned}$$

where $\bar{g}_m(x)$ is a deterministic function and $\zeta_j^{(m)}$, $j \geqslant 0$, are independent and identically distributed Gaussian random variables with zero mean and unit covariance [20].

3. INTERFACIAL FORMULATION

As we now illustrate, the full set of governing equations Eq. (1) can be reformulated entirely in terms of *surface* quantities due to the homogeneous composition of each layer. The advantages of this approach versus the volumetric formulation are obvious in terms of reduced computational resources and accelerated simulation times. Furthermore, as suggested by Kirsch and Monk [30] (see also [31,32]), it is advantageous to accomplish this reformulation in terms of IIOs, as it can be arranged for these to exist for *all* choices of the layer wavenumbers, $k^{(m)}$, in contrast to the DNOs used in alternative formulations [33–35].

To specify the classical IIOs due to Després [36], let $\eta \in \mathbb{R}^+$ define the (lower) surface impedances at $z = a_{m+1} + g_{m+1}(\xi; x)$, $0 \leq m \leq M - 1$,

$$L^{(m)}(\xi; x) := -\frac{\partial v^{(m)}}{\partial \mathbf{n}^{(m+1)}} - i\eta v^{(m)}, \tag{3a}$$

$$\tilde{L}^{(m)}(\xi; x) := -\frac{\partial v^{(m)}}{\partial \mathbf{n}^{(m+1)}} + i\eta v^{(m)}, \tag{3b}$$

and the (upper) surface impedances at $z = a_m + g_m(\xi; x)$, $1 \leq m \leq M$,

$$U^{(m)}(\xi; x) := \frac{\partial v^{(m)}}{\partial \mathbf{n}^{(m)}} - i\eta v^{(m)}, \tag{4a}$$

$$\tilde{U}^{(m)}(\xi; x) := \frac{\partial v^{(m)}}{\partial \mathbf{n}^{(m)}} + i\eta v^{(m)}. \tag{4b}$$

Following [31,32] we now formally define our IIOs and point out that C^2 continuity of the interfaces is certainly enough to justify our statements.

Definition 1 *For $g_1(\xi; x)$ sufficiently smooth, the unique quasiperiodic solution of*

$$\begin{cases} \Delta v^{(0)} + (k^{(0)})^2 v^{(0)} = 0, & (x, z) \in \Omega_0(\xi), \\ \partial_z v^{(0)} - T^{(0)}[v^{(0)}] = 0, & z = a, \\ -\frac{\partial v^{(0)}}{\partial \mathbf{n}^{(1)}} - i\eta v^{(0)} = L^{(0)}, & z = a_1 + g_1(\xi; x), \end{cases} \tag{5}$$

defines the IIO, Q, by $Q[L^{(0)}] := \tilde{L}^{(0)}$.

Definition 2 *For $g_m(\xi; x)$ and $g_{m+1}(\xi; x)$, $1 \le m \le M-1$, sufficiently smooth, the unique quasiperiodic solution of*

$$\begin{cases} \Delta v^{(m)} + (k^{(m)})^2 v^{(m)} = 0, & (x, z) \in \Omega_m(\xi), \\ \frac{\partial v^{(m)}}{\partial \mathbf{n}^{(m)}} - i\eta v^{(m)} = U^{(m)}, & z = a_m + g_m(\xi; x), \\ -\frac{\partial v^{(m)}}{\partial \mathbf{n}^{(m+1)}} - i\eta v^{(m)} = L^{(m)}, & z = a_{m+1} + g_{m+1}(\xi; x), \end{cases} \tag{6}$$

defines the IIO, R, by

$$R^{(m)}\left[\begin{pmatrix} U^{(m)} \\ L^{(m)} \end{pmatrix}\right] = \begin{bmatrix} R^{(m),uu} & R^{(m),ul} \\ R^{(m),lu} & R^{(m),ll} \end{bmatrix} \begin{bmatrix} U^{(m)} \\ L^{(m)} \end{bmatrix} := \begin{bmatrix} \tilde{U}^{(m)} \\ \tilde{L}^{(m)} \end{bmatrix}.$$

Definition 3 *For $g_M(\xi; x)$ sufficiently smooth, the unique quasiperiodic solution of*

$$\begin{cases} \Delta v^{(M)} + (k^{(M)})^2 v^{(M)} = 0, & (x, z) \in \Omega_M(\xi), \\ \frac{\partial v^{(M)}}{\partial \mathbf{n}^{(M)}} - i\eta v^{(M)} = U^{(M)}, & z = a_M + g_M(\xi; x), \\ \partial_z v^{(M)} - T^{(M)}[v^{(M)}] = 0, & z = b, \end{cases} \tag{7}$$

defines the IIO, S, by $S[U^{(M)}] := \tilde{U}^{(M)}$.

Remark 1 *It can be shown that the elliptic boundary value problems* Eq. (5), Eq. (6), *and* Eq. (7) *are all well posed so that all of the IIOs are guaranteed to exist (cf.* [31,32,37]).

By taking appropriate linear combinations of the boundary conditions in Eq. (1), the governing equations can be written as

$$A\mathbf{x} = \mathbf{b}, \tag{8}$$

in terms of the impedances, $\{L, U\}$, which appear in $\mathbf{x}$, and the IIOs described above, which feature in A. (We note that the incident radiation is found in the right-hand side $\mathbf{b}$.) Furthermore, due to the well-posedness of the problems Eq. (5), Eq. (6), and Eq. (7), the full system of equations, Eq. (1), is equivalent to this interfacial formulation, Eq. (8). Please refer to Section 1 of Supplement 1 for full details.

Remark 2 *We point out that the choice of surface unknowns in* Eq. (3) *and* Eq. (4) *was made for mathematical reasons: They deliver well-defined operators (IIOs) throughout the spectrum of illumination frequencies. Such choices are commonplace in the non-overlapping domain decomposition literature* [32], *which studies iteration schemes for solving the scattering problem* Eq. (1) *where one set of transmission variables, e.g., $\{\tilde{L}^{(m)}, \tilde{U}^{(m)}\}$, is used to update the others, say, $\{L^{(m)}, U^{(m)}\}$. It can be shown that in the one-dimensional case this iteration scheme will converge in a finite number of steps if one chooses $\eta = k^{(m)}$ (in fact, the speed of light is typically rescaled to unity so that $\eta = \omega$ is chosen)* [32]. *In higher dimensions, the analysis is more subtle, and convergence in a finite number of steps cannot be guaranteed, but optimal convergence rates are typically found when η is chosen to be a small deviation from $k^{(m)}$. Our nomenclature of the surface quantities as "impedances" follows that in* [31] *where the authors judged this to be superior to "transmission variables" or "Robin variables." While the quantities in* Eq. (3) *and* Eq. (4) *resemble physical quantities, they do not generically have physical significance.*

With this surface reformulation in place, all that remains to be specified is how the IIOs (Q, R, S) are to be computed. All of the classical volumetric approaches are available for this including the finite difference method [38], the finite element method [39], the discontinuous Galerkin method [40], the spectral element method [41], and the spectral method [21,22] to name a few. However, due to the homogeneous nature of the material layers, a surface method will be greatly advantaged, and so we pursue this here. While integral equation methods are popular choices for this [42], we advocate a HOPS approach due to the parameterized nature of the interfaces. More specifically, we now describe a TFE method [43] for this computation.

A. Method of Transformed Field Expansions

Following [20,43], the TFE approach to simulating our IIOs begins with a domain-flattening change of variables. This new set of coordinates, first introduced by Phillips [44] and later Chandezon [45], stabilizes the closely related field expansions (FE) method devised by Bruno and Reitich [46], which will be crucial in our simulations.

To begin, for each sample ξ, we consider the new coordinates $x' = x$ and, in each layer ($0 \le m \le M$),

$$z' = a_{m+1}\left(\frac{(a_m + g_m(\xi; x)) - z}{h^{(m)} + g_m(\xi; x) - g_{m+1}(\xi; x)}\right) + a_m\left(\frac{z - (a_{m+1} + g_{m+1}(\xi; x))}{h^{(m)} + g_m(\xi; x) - g_{m+1}(\xi; x)}\right),$$

where $h^{(m)} := a_m - a_{m+1}$, $\{a_0 = a, g_0 \equiv 0\}$, and $\{a_{M+1} = b, g_{M+1} \equiv 0\}$. Next, we define the transformed fields

$$w^{(m)}(\xi; x', z') := v^{(m)}(\xi; x(x', z'), z(x', z')),$$

for $0 \le m \le M$.

For brevity we now focus upon the computation of the inner-layer IIO, $R^{(m)}$, for any $1 \le m \le M-1$, and note that similar considerations apply to the upper- and lower-layer IIOs, S and Q. By the above change of variables, a straightforward calculation shows that under the new coordinates, the governing equations Eq. (6) become

$$\begin{cases} \Delta' w^{(m)} + (k^{(m)})^2 w^{(m)} = F^{(m)}, & a_{m+1} < z' < a_m, \\ \partial_{z'} w^{(m)} - i\eta w^{(m)} = U^{(m)} + J^{(m),u}, & z' = a_m, \\ -\partial_{z'} w^{(m)} - i\eta w^{(m)} = L^{(m)} + J^{(m),l}, & z' = a_{m+1}, \end{cases} \tag{9}$$

and the IIO satisfies

$$\begin{bmatrix} R^{(m),u}[U^{(m)}, L^{(m)}] \\ R^{(m),l}[U^{(m)}, L^{(m)}] \end{bmatrix} = \begin{bmatrix} (\partial_{z'} w^{(m)} + i\eta w^{(m)})\big|_{z'=a_m} \\ (-\partial_{z'} w^{(m)} + i\eta w^{(m)})\big|_{z'=a_{m+1}} \end{bmatrix} + \begin{bmatrix} K^{(m),u} \\ K^{(m),l} \end{bmatrix}. \tag{10}$$

We refer the reader to Section 2 of Supplement 1 for a detailed description of the functions $F^{(m)}$, $J^{(m),u}$, $J^{(m),l}$, $K^{(m),u}$, and $K^{(m),l}$. Importantly, each depends at least linearly on g_m so that, if $g_m = \varepsilon \tilde{g}_m$, then each of these is $\mathcal{O}(\varepsilon)$.

Next, we recall that we have parameterized the layer interfaces by ε and seek a solution of our *transformed* governing equations, Eq. (9), in a Taylor series

$$w^{(m)} = w^{(m)}(\xi; x', z'; \varepsilon) = \sum_{n=0}^{\infty} w_n^{(m)}(\xi; x', z')\varepsilon^n. \tag{11}$$

Given the known impedances

$$L^{(m)}(\xi; x; \varepsilon) = \sum_{n=0}^{\infty} L_n^{(m)}(\xi; x)\varepsilon^n,$$

$$U^{(m)}(\xi; x; \varepsilon) = \sum_{n=0}^{\infty} U_n^{(m)}(\xi; x)\varepsilon^n,$$

we can uniquely solve Eq. (9) and express the IIOs as

$$\begin{pmatrix} R^{(m),u}[U^{(m)}, L^{(m)}] \\ R^{(m),l}[U^{(m)}, L^{(m)}] \end{pmatrix} = \sum_{n=0}^{\infty} \begin{pmatrix} R_n^{(m),u}[U^{(m)}, L^{(m)}] \\ R_n^{(m),l}[U^{(m)}, L^{(m)}] \end{pmatrix} \varepsilon^n.$$

Upon inserting the expansion Eq. (11) for w into the (transformed) governing equations, Eq. (9), we find

$$\begin{cases} \Delta' w_n^{(m)} + (k^{(m)})^2 w_n^{(m)} = F_n^{(m)}, \ a_{m+1} < z' < a_m, \\ \partial_{z'} w_n^{(m)} - i\eta w_n^{(m)} = U_n^{(m)} + J_n^{(m),u}, \ z' = a_m, \\ -\partial_{z'} w_n^{(m)} - i\eta w_n^{(m)} = L_n^{(m)} + J_n^{(m),l}, \ z' = a_{m+1}, \end{cases} \tag{12}$$

and, from Eq. (11) placed in Eq. (10),

$$\begin{bmatrix} R_n^{(m),u}[U^{(m)}, L^{(m)}] \\ R_n^{(m),l}[U^{(m)}, L^{(m)}] \end{bmatrix} = \begin{bmatrix} (\partial_{z'} w_n^{(m)} + i\eta w_n^{(m)})\big|_{z'=a_m} \\ (-\partial_{z'} w_n^{(m)} + i\eta w_n^{(m)})\big|_{z'=a_{m+1}} \end{bmatrix} + \begin{bmatrix} K_n^{(m),u} \\ K_n^{(m),l} \end{bmatrix}. \tag{13}$$

Here we use the convention that $w_n^{(m)} \equiv 0$ if $n < 0$. We refer the reader to Section 3 of Supplement 1 for a detailed description of the functions $F_n^{(m)}$, $J_n^{(m),u}$, $J_n^{(m),l}$, $K_n^{(m),u}$, and $K_n^{(m),l}$.

With this HOPS approach in mind, we point out that our full set of governing equations, Eq. (8), can be written as

$$A(\varepsilon)\mathbf{x}(\varepsilon) = \mathbf{b}(\varepsilon),$$

which, upon Taylor expansion, reads

$$\left(\sum_{n=0}^{\infty} A_n \varepsilon^n\right)\left[\sum_{n=0}^{\infty} \mathbf{x}_n \varepsilon^n\right] = \sum_{n=0}^{\infty} \mathbf{b}_n \varepsilon^n.$$

Equating at each order $n \geqslant 0$, one discovers a formula for $\mathbf{x}_n$

$$A_0 \mathbf{x}_n = \mathbf{b}_n - \sum_{r=0}^{n-1} A_{n-r}\mathbf{x}_r. \tag{14}$$

From this it is clear that the key to this regular perturbation approach is the linear operator A_0 and its inverse. As described in Section 3 of Supplement 1, this operator is composed of the order-zero (infinitesimal) IIOs, which we presently investigate.

Remark 3 *The flat-interface case is addressed by* Eq. (14) *with* $\varepsilon = 0$ *corresponding to* $A_0\mathbf{x}_0 = \mathbf{b}_0$. *This equation is equivalent to the classical Fresnel equation* [26], *which delivers the transmission and reflection coefficients in a multiply layered medium with flat interfaces. To see this, one must use the inversion formulas*

$$\frac{\partial v^{(m)}}{\partial \mathbf{n}^{(m+1)}} = -\frac{1}{2}\left\{L^{(m)} + \tilde{L}^{(m)}\right\}, \quad v^{(m)} = \frac{1}{2i\eta}\left\{\tilde{L}^{(m)} - L^{(m)}\right\},$$

and

$$\frac{\partial v^{(m)}}{\partial \mathbf{n}^{(m)}} = -\frac{1}{2}\left\{U^{(m)} + \tilde{U}^{(m)}\right\}, \quad v^{(m)} = \frac{1}{2i\eta}\left\{\tilde{U}^{(m)} - U^{(m)}\right\},$$

which can be derived by adding and subtracting the equations in Eq. (3) *and* Eq. (4), *respectively. From these physically relevant quantities (the surface field* $v^{(m)}$ *and surface curren,* $\partial v^{(m)}/\partial \mathbf{n}^{(m)}$*) one can readily recover the reflection and transmission coefficients once it is observed that, due to the plane-wave incidence and the flat interfaces, this system of equations need only be solved at wavenumber* $p = 0$.

B. IIO on a Domain with Infinitesimal Deformations

We have just observed that the crucial consideration in our HOPS approach is the order-zero operator, A_0, which features the order-zero IIOs, Q_0, $R_0^{(m)}$, and S_0. Again we fix upon the inner layer case and recover an explicit form for $R_0^{(m)}$ by using the fact that the order-zero problem corresponds to the IIO problem on a domain with infinitesimal (vanishing) boundary perturbations. More specifically we consider Eq. (12) at $n = 0$:

$$\begin{cases} \Delta' w_0^{(m)} + (k^{(m)})^2 w_0^{(m)} = 0, \ a_{m+1} < z' < a_m, \\ \partial_{z'} w_0^{(m)} - i\eta w_0^{(m)} = U_0^{(m)}, \ z' = a_m, \\ -\partial_{z'} w_0^{(m)} - i\eta w_0^{(m)} = L_0^{(m)}, \ z' = a_{m+1}. \end{cases} \tag{15}$$

Before proceeding we make a trivial change of variables that simply shifts the domain $\{a_{m+1} < z' < a_m\}$ to $\{-h < \tilde{z} < h\}$, namely, $\tilde{x} = x'$ and

$$\tilde{z} = -h\left\{\frac{a_m - z'}{a_m - a_{m+1}}\right\} + h\left(\frac{z' - a_{m+1}}{a_m - a_{m+1}}\right),$$

where $h = (a_m - a_{m+1})/2$. If we let

$$u_0^{(m)}(\tilde{x}, \tilde{z}) := w_0^{(m)}(x'(\tilde{x}, \tilde{z}), z'(\tilde{x}, \tilde{z})),$$

then Eq. (15) becomes

$$\begin{cases} \tilde{\Delta} u_0^{(m)} + (k^{(m)})^2 u_0^{(m)} = 0, \ -h < \tilde{z} < h, \\ \partial_{\tilde{z}} u_0^{(m)} - i\eta u_0^{(m)} = U_0^{(m)}, \ \tilde{z} = h, \\ -\partial_{\tilde{z}} u_0^{(m)} - i\eta u_0^{(m)} = L_0^{(m)}, \ \tilde{z} = -h. \end{cases}$$

The solutions of the Helmholtz equation are

$$u_0^{(m)} = \sum_{p=-\infty}^{\infty} \left(a_p^{(m)} \cosh(i\gamma_p^{(m)}\tilde{z}) + b_p^{(m)} \frac{\sinh(i\gamma_p^{(m)}\tilde{z})}{i\gamma_p^{(m)}} \right) e^{i\alpha_p \tilde{x}},$$

while the boundary conditions give the following linear system

$$\begin{bmatrix} a_{m,p} & b_{m,p} \\ a_{m,p} & -b_{m,p} \end{bmatrix} \begin{bmatrix} a_p^{(m)} \\ b_p^{(m)} \end{bmatrix} = \begin{bmatrix} \hat{U}_{0,p}^{(m)} \\ \hat{L}_{0,p}^{(m)} \end{bmatrix}; \tag{16}$$

formulas for the entries are specified in Section 4 of Supplement 1. It can be shown that this system has a unique solution that we now utilize to discover a form for the pth Fourier coefficient of $R_0^{(m)}$:

$$R_{0,p}^{(m)} \begin{bmatrix} \hat{U}_{0,p}^{(m)} \\ \hat{L}_{0,p}^{(m)} \end{bmatrix} = \begin{bmatrix} \bar{a}_{m,p} & \bar{b}_{m,p} \\ \bar{a}_{m,p} & -\bar{b}_{m,p} \end{bmatrix} \begin{bmatrix} a_{m,p} & b_{m,p} \\ a_{m,p} & -b_{m,p} \end{bmatrix}^{-1} \begin{bmatrix} \hat{U}_{0,p}^{(m)} \\ \hat{L}_{0,p}^{(m)} \end{bmatrix}.$$

It is not difficult to see that

$$R_{0,p}^{(m)} = \frac{1}{2} \begin{bmatrix} \frac{\bar{a}_{m,p}}{a_{m,p}} + \frac{\bar{b}_{m,p}}{b_{m,p}} & \frac{\bar{a}_{m,p}}{a_{m,p}} - \frac{\bar{b}_{m,p}}{b_{m,p}} \\ \frac{\bar{a}_{m,p}}{a_{m,p}} - \frac{\bar{b}_{m,p}}{b_{m,p}} & \frac{\bar{a}_{m,p}}{a_{m,p}} + \frac{\bar{b}_{m,p}}{b_{m,p}} \end{bmatrix},$$

which is readily verified to be unitary so that its inverse is its conjugate transpose. Furthermore, it has been shown [25,31,32,47] that the operator $R^{(m)}$ is still unitary for nonzero boundary deformations indicating that its computation will be well-conditioned.

C. Reduction to Two-Point Boundary Value Problems

As both the fields $w^{(m)}$ and their nth order Taylor corrections are quasiperiodic in the lateral variable we may expand them in generalized Fourier (Floquet) series

$$w_n^{(m)}(\xi; , x', z'; \varepsilon) = \sum_{p=-\infty}^{\infty} \hat{w}_{n,p}^{(m)}(\xi; z') e^{i\alpha_p x'}.$$

Expanding the impedance data in a similar fashion,

$$L_n^{(m)}(\xi; , x') = \sum_{p=-\infty}^{\infty} \hat{L}_{n,p}^{(m)} e^{i\alpha_p x'},$$

and

$$U_n^{(m)}(\xi; , x') = \sum_{p=-\infty}^{\infty} \hat{U}_{n,p}^{(m)} e^{i\alpha_p x'},$$

and we may insert these forms into Eq. (12) to realize, at each wavenumber p, the two-point boundary value problems

$$\begin{cases} \partial_{z'}^2 \hat{w}_{n,p}^{(m)} + (\gamma_p^{(m)})^2 \hat{w}_{n,p}^{(m)} = F_{n,p}^{(m)}, & a_{m+1} < z' < a_m, \\ \partial_{z'} \hat{w}_{n,p}^{(m)} - i\eta \hat{w}_{n,p}^{(m)} = \hat{U}_{n,p}^{(m)} + J_{n,p}^{(m),l}, & z' = a_m, \\ -\partial_{z'} \hat{w}_{n,p}^{(m)} - i\eta \hat{w}_{n,p}^{(m)} = \hat{L}_{n,p}^{(m)} + J_{n,p}^{(m),l}, & z' = a_{m+1}. \end{cases} \tag{17}$$

We note that for each random sample ξ and for each Taylor order n, we have the same deterministic differential operator on the left-hand side of Eq. (17), which we will presently use to great effect in our numerical algorithm [20,27].

4. NUMERICAL ALGORITHM

At this point we can specify a rapid, accurate, and robust numerical procedure for the simulation of scattering by random diffraction gratings that satisfy Eq. (1), reformulated in terms of interfacial unknowns and IIOs, Eq. (8), the latter of which are computed by the TFE method.

A. Fourier–Chebyshev–Taylor Collocation Method

The only difficult aspect of our numerical algorithm is the TFE method applied to the IIO problems, Eq. (9) and Eq. (10), and for this we approximate the fields $w^{(m)}$ with a Fourier–Chebyshev–Taylor form

$$w^{(m)}(\xi; x', z'; \varepsilon) \approx \sum_{n=0}^{N} \sum_{p=-N_x/2}^{N_x/2-1} \sum_{l=0}^{N_z} \hat{w}_{n,p,l}^{(m)} e^{i\alpha_p x'} T_l\left(\tfrac{2z'-a_m-a_{m+1}}{a_m-a_{m+1}} \right) \varepsilon^n,$$

where T_l is the lth Chebyshev polynomial [21,25]. To specify equations for the $\hat{w}_{n,p,l}^{(m)}$, we begin by defining the N_x Fourier collocation points

$$x_j' = \frac{dj}{N_x}, \quad 0 \le j \le N_x - 1,$$

in the lateral (x) direction, and the $N_z + 1$ Chebyshev collocation points

$$z_l' = \left(\frac{a_m - a_{m+1}}{2} \right) \left(\cos\left(\frac{l\pi}{N_z} \right) - 1 \right) + a_m, \quad 0 \le l \le N_z,$$

in the vertical (z) direction. We point out that the latter have been transformed from the standard interval, $[-1, 1]$, to $[a_{m+1}, a_m]$ of interest to us. To find the unknowns $\hat{w}_{n,p,l}^{(m)}$ in an internal layer $1 \le m \le M-1$, for instance, we demand that the equation Eq. (17) be true at the collocation points (x_j', z_l') for each perturbation order $0 \le n \le N$ and at each of R-many Monte Carlo samples, ξ_r, $0 \le r \le R$. This results in the linear algebra problem

$$A_p^{(m)} \tilde{\mathbf{w}}_{n,p}^{(m)} = \tilde{\mathbf{f}}_{n,p}^{(m)}, \quad \tilde{\mathbf{w}}_{n,p}^{(m)}, \tilde{\mathbf{f}}_{n,p}^{(m)} \in \mathbb{C}^{N_z+1}, \tag{18}$$

and

$$A_p^{(m)} = \left\{ \left(\frac{2}{h} D_{N_z} \right)^2 + (\gamma_p^{(m)})^2 I \right\} \in \mathbb{C}^{(N_z+1)\times(N_z+1)},$$

where D_{N_z} is the Chebyshev differentiation matrix [23] and I is the $(N_z+1) \times (N_z+1)$ identity matrix. Please refer to Section 5 of Supplement 1 for more detailed descriptions of the discretized problems in each layer.

Of crucial importance is the fact that the matrix $A_p^{(m)}$ is *deterministic* (independent of the sample ξ) and can be computed and factored *once* for each wavenumber p. In this way the dominant cost of our Monte Carlo sampling strategy can be significantly reduced by simply storing the resulting N_x-many LU factorizations and reusing them for each sample and perturbation order.

B. Monte Carlo Sampling and Computational Complexity

To investigate the probability space of random interfaces, we use the Monte Carlo sampling. For a (large) number of random samples, the boundary value problem, Eq. (1), is solved for each realization generated, and the statistics (mean and variance) of the solution are computed. The Monte Carlo method is quite simple but also very slow with a convergence rate $\mathcal{O}(\sqrt{R})$ for R samples [48]. The decision to use Monte Carlo sampling in our numerical algorithm was made for reasons of simplicity and clarity of presentation. However, it is important to note that more efficient sampling techniques could be used, e.g., quasi-Monte Carlo methods [48], coupled to variance reduction techniques [29]. We view each of these as avenues of future research on this topic.

In light of our observation that the discrete differential operator $A^{(m)}_{n,p}$ can be formed, and LU factorized and stored once for each choice of wavenumber p, the computational complexity of the whole numerical algorithm is $\mathcal{O}(RN_xN_z^2N^2)$ by applying forward and backward substitutions to obtain the solution of Eq. (18) for each sample ξ and each perturbation order n. This yields significant reduction in computational cost compared to $\mathcal{O}(RN_xN_z^3N^2)$ computational complexity if this realization is not made.

5. NUMERICAL RESULTS

At this point we can present numerical results to demonstrate the stability and accuracy of our numerical algorithm as measured by the mean and variance of the energy defect, $\bar{e}$ and σ_e^2, respectively. In a grating scattering problem the principle of conservation of energy states that the (scaled) total energy, reflected plus transmitted, must be unity [26]. Thus, we can express a measure of deviation from this law with the "energy defect"

$$e(\xi) := \sum_{p\in P^{(0)}} \frac{\gamma_p^{(0)}}{\gamma_0^{(0)}} \left| \sum_{n=0}^{\infty} \hat{w}_{n,p}^{(0)}(\xi; a)\varepsilon^n \right|^2 + \sum_{p\in P^{(M)}} \frac{\gamma_p^{(M)}}{\gamma_0^{(0)}} \left| \sum_{n=0}^{\infty} \hat{w}_{n,p}^{(M)}(\xi; b)\varepsilon^n \right|^2 - 1, \tag{19}$$

which, in the absence of approximation, should be zero.

For our tests we considered three-layer structures, featuring $M = 2$ random interfaces, and restricted our attention to TE polarization. The electromagnetic parameters were chosen to be

$$k^{(0)} = 2\pi, \quad k^{(1)} = \pi, \quad k^{(2)} = 2\pi,$$

while we considered the geometric quantities

$$a = 1.1, \quad b = -1.1, \quad d = 9, \quad 2h = 2.2.$$

Electromagnetic radiation of normal incidence ($\theta = 0$) was used to illuminate the structure for each of $R = 10^4$ Monte Carlo samples. Initially Taylor summation was used to approximate the truncated Taylor series, though, as we shall describe, comparisons with Padé summation were also made. In the following results we denote by ϵ_{mach} machine zero in IEEE double precision (roughly 2.2×10^{-16}).

A. Varying the Lateral and Horizontal Discretization

We began our experiments by varying the lateral and horizontal discretizations, N_x and N_z, while leaving the correlation length, perturbation size, and number of Taylor orders fixed at $l_c = 1$, $\varepsilon = 0.1$, and $N = 20$, respectively. From Tables 1 and 2 we can clearly observe the robust convergence of the mean and variance of the energy defect as the discretization parameters, N_x and N_z, are refined. Furthermore, this rate of convergence is exponential (down to machine zero) as one would expect from our Fourier–Chebyshev approach.

B. Varying the Perturbation Size and Number of Taylor Orders

We continued by varying the perturbation size ε and number of Taylor orders N, while leaving the correlation length and lateral/vertical discretizations fixed at $l_c = 1$ and $N_x = N_z = 2^5$, respectively. Tables 3 and 4 clearly demonstrate the stable convergence of the mean and variance of the energy defect for assorted values of the perturbation size ε as the number of Taylor orders N is refined. Furthermore, as Fig. 2 displays, this rate of convergence is exponential (down to machine zero) as one would expect from our Taylor approach, and this rate improves for smaller deformations ε.

C. Padé versus Taylor Summation

It has been observed in previous research on HOPS schemes [43] that, while the disk of analyticity of the series Eq. (11) is of finite radius, it includes a neighborhood of the *entire* real axis (up to topological obstruction). For our numerical simulations this has the effect that, for large values of ε, Taylor summation fails. However, numerical analytic continuation techniques *can* access this domain of extended analyticity, and Padé summation has proven useful for this task. We recall that, given a function

Table 1. Absolute Value of the Mean of the Energy Defect $|\bar{e}|$ as the Lateral (N_x) and Vertical (N_z) Discretizations Were Refined[a]

N_x	$N_z = 2^3$	$N_z = 2^4$	$N_z = 2^5$	$N_z = 2^6$
2^3	1.0501e-03	1.0814e-03	1.0802e-03	1.0827e-03
2^4	3.8155e-05	1.1569e-06	1.1161e-06	1.1277e-06
2^5	3.9156e-05	5.3976e-10	5.5434e-10	5.5156e-10
2^6	3.9349e-05	1.1695e-11	2.3820e-13	2.4384e-13

[a]Correlation length, perturbation size, and number of Taylor orders fixed at $l_c = 1$, $\varepsilon = 0.1$, and $N = 20$, respectively.

Table 2. Standard Deviation of the Energy Defect σ_e^2 as the Lateral (N_x) and Vertical (N_z) Discretizations Were Refined[a]

N_x	$N_z = 2^3$	$N_z = 2^4$	$N_z = 2^5$	$N_z = 2^6$
2^3	1.8407e-06	1.8379e-06	1.8221e-06	1.8365e-06
2^4	1.4026e-08	8.6896e-10	8.6678e-10	8.6775e-10
2^5	1.2821e-08	ϵ_{mach}	ϵ_{mach}	ϵ_{mach}
2^6	1.2812e-08	ϵ_{mach}	ϵ_{mach}	ϵ_{mach}
2^7	1.2818e-08	ϵ_{mach}	ϵ_{mach}	ϵ_{mach}

[a]Correlation length, perturbation size, and number of Taylor orders fixed at $l_c = 1$, $\varepsilon = 0.1$, and $N = 20$, respectively.

Table 3. Absolute Value of the Mean of the Energy Defect $|\bar{e}|$ as the Number of Taylor Orders N Was Varied for Assorted Values of the Perturbation Size ε[a]

ε	$N=2$	$N=4$	$N=8$	$N=16$
0.01	2.5860e-07	8.9270e-11	5.8876e-12	5.8876e-12
0.05	1.8107e-04	1.8469e-06	4.0214e-09	3.9343e-09
0.1	2.8511e-03	1.0254e-04	1.3407e-07	6.2869e-08
0.2	4.6765e-02	3.2213e-03	2.5526e-05	4.6869e-06

[a]Correlation length and lateral/vertical discretization fixed at $l_c = 1$ and $N_x = N_z = 2^5$, respectively.

Table 4. Standard Deviation of the Energy Defect σ_e^2 as the Number of Taylor Orders N Was Varied for Assorted Values of the Perturbation Size ε[a]

ε	$N=2$	$N=4$	$N=8$	$N=16$
0.01	1.5934e-11	$\varepsilon_{\text{mach}}$	$\varepsilon_{\text{mach}}$	$\varepsilon_{\text{mach}}$
0.05	2.8624e-07	1.0078e-10	1.4301e-16	1.3036e-16
0.1	2.9170e-05	1.2568e-07	2.7749e-12	1.3858e-14
0.2	5.1089e-03	1.1718e-04	3.9580e-07	7.0365e-08

[a]Correlation length and lateral/vertical discretization fixed at $l_c = 1$ and $N_x = N_z = 2^5$, respectively.

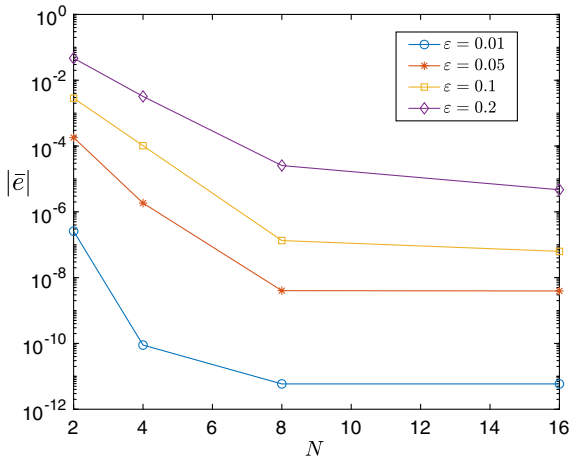

Fig. 2. Plot of the absolute value of the mean of the energy defect $|\bar{e}|$ as the number of Taylor orders N was varied for assorted values of the perturbation size ε. Correlation length and lateral/vertical discretization fixed at $l_c = 1$ and $N_x = N_z = 2^5$, respectively.

$$f(z) = \sum_{n=0}^{\infty} c_n \varepsilon^n,$$

the truncated Taylor series works magnificently in approximating $f(z)$ at points of analyticity inside the disk of convergence. The Padé approximant provides a means for approximating $f(z)$ at points of analyticity that are outside the disk of convergence of the Taylor series [49]. The Padé approximant is defined as the rational function

$$[L/M](z) := \frac{\sum_{l=0}^{L} a_l z^l}{1 + \sum_{m=1}^{M} b_m z^m},$$

where

Table 5. Absolute Value of the Mean of the Energy Defect $|\bar{e}|$ as the Number of Taylor Orders N Was Varied for Assorted Values of the Perturbation Size ε Calculated via Taylor Summation[a]

ε	$N=2^3$	$N=2^4$	$N=2^5$	$N=2^6$
0.1	7.8669e-08	9.5712e-09	9.6114e-09	9.6099e-09
0.2	2.4983e-05	5.4705e-06	1.3548e-08	1.4908e-07
0.4	4.0993e-01	1.6469e+03	2.3238e+11	1.5042e+28

[a]Correlation length and lateral/vertical discretization fixed at $l_c = 1$ and $N_x = N_z = 2^6$, respectively.

Table 6. Absolute Value of the Mean of the Energy Defect $|\bar{e}|$ as the Number of Taylor Orders N Was Varied for Assorted Values of the Perturbation Size ε Calculated via Padé Summation[a]

ε	$N=2^3$	$N=2^4$	$N=2^5$	$N=2^6$
0.1	6.9990e-09	9.5992e-09	9.6114e-09	9.6099e-09
0.2	2.5644e-06	1.3940e-07	1.3943e-07	1.3987e-07
0.4	1.2791e-03	2.3498e-06	1.7707e-06	1.7775e-06
0.6	2.5179e-02	1.8212e-04	6.7339e-06	6.5450e-06
0.8	1.2679e-01	8.4429e-03	1.6977e-05	2.0144e-05
1	3.6152e-01	1.1361e-01	2.6508e-03	1.5363e-03
1.1	9.3667e-01	9.3128e-01	1.0762e-02	6.0850e-03
1.2	1.6302	0.9515	0.0654	3.2271e-02

[a]Correlation length and lateral/vertical discretization fixed at $l_c = 1$ and $N_x = N_z = 2^6$, respectively.

$$[L/M](z) = \sum_{n=0}^{N} c_n z^n + \mathcal{O}(z^{L+M+1}), \quad L + M = N.$$

In particular, we considered the equi-order Padé approximant $[M/M](z)$, where, for simplicity, we assumed that N is even (so that $M = N/2$). We point out the work [49–51] as excellent sources of information on Padé approximation, including convergence results for the equi-order Padé approximants.

To showcase the capabilities of Padé approximation in the current context, we revisited the calculations of the previous section for much larger values of the interface perturbation ε. All parameter values considered above were used again, save (i) $N_x = N_z$ was increased slightly to 2^6 and (ii) for $\varepsilon < 1$, we selected $a = -b = 2.1$, while, for $\varepsilon > 1$, we set $2h = 3.2$ and chose $a = -b = 4.1$. The results given in Table 5 demonstrate not only the convergence of Taylor summation for $\varepsilon = 0.1, 0.2$ (inside the disk of analyticity), but also its spectacular failure at the value $\varepsilon = 0.4$ (clearly outside the disk of analyticity). However, the data in Table 6 show that with Padé summation, not only can excellent results be realized for this bigger value of $\varepsilon = 0.4$, but also that meaningful results can be deduced for the *much* larger values of $\varepsilon = 1.1$ and even 1.2. These results are reinforced in Fig. 3, showing the divergence of our results with Taylor summation outside the disk of analyticity, and Fig. 4, which displays the enhancing effects of Padé approximation.

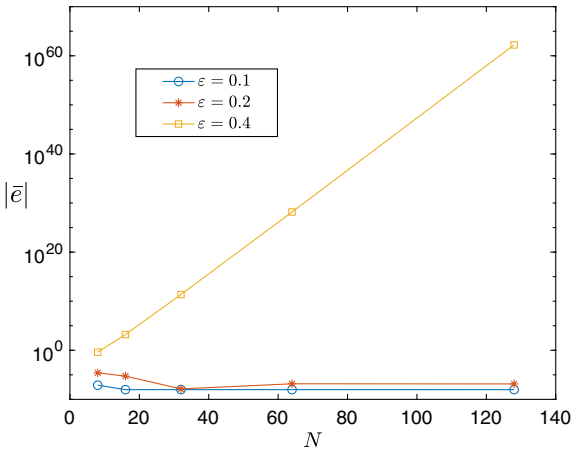

Fig. 3. Plot of the absolute value of the mean of the energy defect $|\bar{e}|$ as the number of Taylor orders N was varied for assorted values of the perturbation size ε calculated via Taylor summation. Correlation length and lateral/vertical discretization fixed at $l_c = 1$ and $N_x = N_z = 2^6$, respectively.

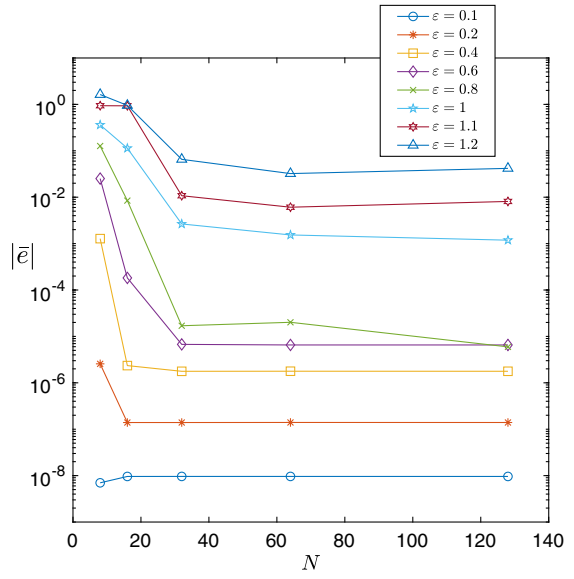

Fig. 4. Plot of the absolute value of the mean of the energy defect $|\bar{e}|$ as the number of Taylor orders N was varied for assorted values of the perturbation size ε calculated via Padé summation. Correlation length and lateral/vertical discretization fixed at $l_c = 1$ and $N_x = N_z = 2^6$, respectively.

D. Plots of the Total Field for a Fixed Random Sample

We close with plots of the total field in the top, middle, and bottom layers, which are calculated and plotted in the original coordinates $(x(x', z'), z(x', z'))$ for a fixed random sample. The electromagnetic parameters and the geometric quantities stated at the beginning of Section 5 (with the exception of the artificial boundaries, which were set to $a = 2.1$ and $b = 2.1$) along with $\varepsilon = 0.1$, $N_x = 2^6$, $N_z = 2^6$, $N = 10$, and $l_c = 1$ were used in the calculations of the total fields.

Recall that the total field is denoted by v and that the transformed fields are defined by

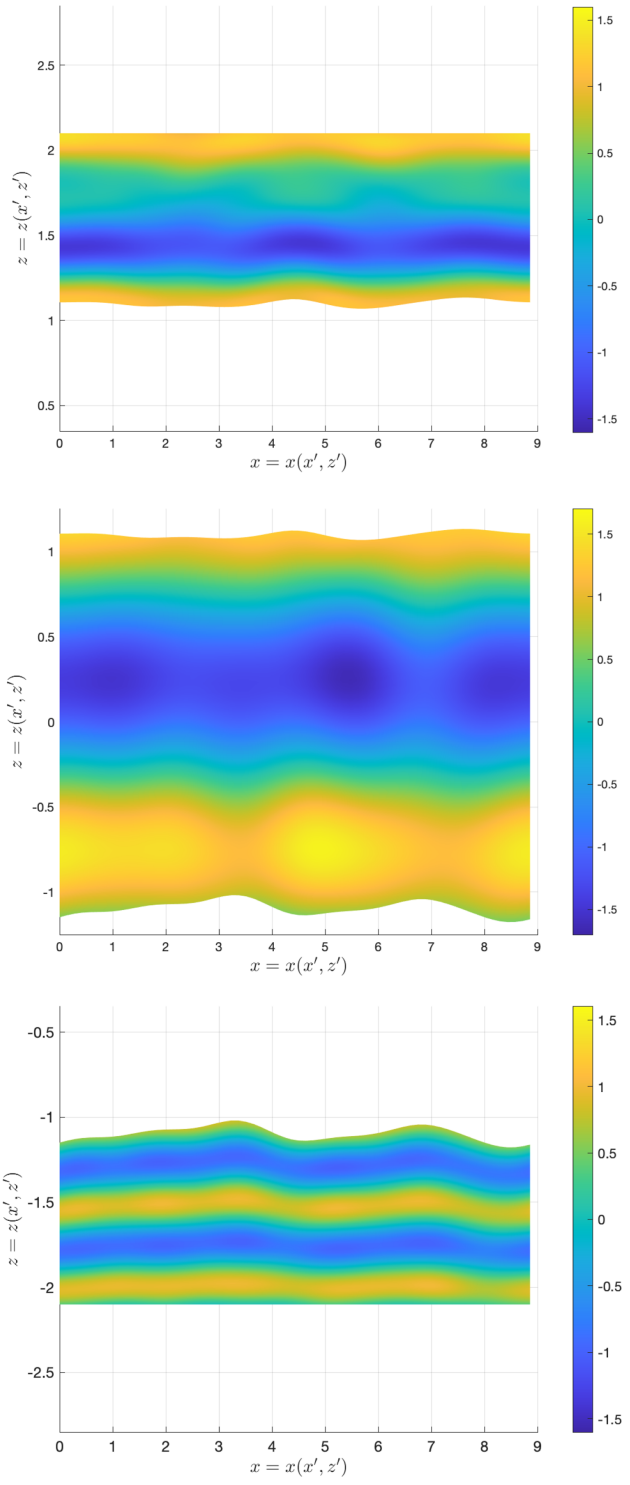

Fig. 5. Plot of the total field in the top $(v = v^{(0)} + v^{\text{inc}})$, middle $(v = v^{(1)})$, and bottom $(v = v^{(2)})$ layers, respectively, in original coordinates, for the fixed random sample. The lateral discretization, vertical discretization, and Taylor order were fixed at $N_x = 2^6$, $N_z = 2^6$, and $N = 10$, respectively. The deformation parameter, period, and correlation length are set to $\varepsilon = 0.1$, $d = 9$, and $l_c = 1$, respectively.

$$w^{(m)}(\xi; x', z') := v^{(m)}(\xi; x(x', z'), z(x', z'))$$

for $m = 0, \ldots, M$. From top to bottom, Fig. 5 displays the total field in the top layer $(v = v^{\text{inc}} + v^{(0)})$, middle layer

($v = v^{(1)}$), and bottom layer ($v = v^{(2)}$), respectively, in the original coordinates for the fixed random sample.

6. CONCLUSION

We have presented a novel numerical method to efficiently and accurately model the scattering of electromagnetic fields by mulitply layered gratings with random interfaces. The components of this algorithm, the MCTFE method, are (i) an interfacial problem formulation in terms of IIO, (ii) simulated by a HOPS approach (the TFE method), (iii) coupled to efficient Monte Carlo sampling. Our high-order perturbative formulation permits us to solve a sequence of linear problems featuring an operator that is *deterministic*, which leads to significant savings in computational effort. Through numerical examples we demonstrated not only the robust and high-order accuracy of our scheme for gratings with small to moderate interface deformations, but also how Padé summation could be used to address layer shapes that are large deviations from the base, flat-interface configuration.

Funding. National Science Foundation (DMS-1719851, DMS-1813033, DMS-2011148, DMS-2111283).

Disclosures. The authors declare no conflict of interest.

Data availability. No data were generated or analyzed in the presented research.

Supplemental document. See Supplement 1 for supporting content.

REFERENCES

1. A. K. Fung, Z. Li, and K. S. Chen, "Backscattering from a randomly rough dielectric surface," IEEE Trans. Geosci. Remote Sens. **30**, 356–369 (1992).
2. L. Tsang, J. A. Kong, and R. T. Shin, *Theory of Microwave Remote Sensing* (Wiley, 1985).
3. B. Lin, S. J. Katzberg, J. L. Garrison, and B. A. Wielicki, "Relationship between GPS signals reflected from sea surfaces and surface winds: modeling results and comparisons with aircraft measurements," J. Geophys. Res. Oceans **104**, 20713–20727 (1999).
4. D. R. Thompson, T. M. Elfouhaily, and J. L. Garrison, "An improved geometrical optics model for bistatic GPS scattering from the ocean surface," IEEE Trans. Geosci. Remote Sens. **43**, 2810–2821 (2005).
5. J. V. Coe, J. M. Heer, S. Teeters-Kennedy, H. Tian, and K. R. Rodriguez, "Extraordinary transmission of metal films with arrays of subwavelength holes," Ann. Rev. Phys. Chem. **59**, 179–202 (2008).
6. J. Homola, "Surface plasmon resonance sensors for detection of chemical and biological species," Chem. Rev. **108**, 462–493 (2008).
7. M. Moskovits, "Surface–enhanced spectroscopy," Rev. Mod. Phys. **57**, 783–826 (1985).
8. D. P. Nicholls, F. Reitich, T. W. Johnson, and S. H. Oh, "Fast high-order perturbation of surfaces methods for simulation of multilayer plasmonic devices and metamaterials," J. Opt. Soc. Am. A **31**, 1820–1831 (2014).
9. G. Bao, Y. Cao, J. Lin, and H.-W. van Wyk, "Computational optimal design of random rough surfaces in thin-film solar cells," Commun. Comput. Phys. **25**, 1591–1612 (2019).
10. P. Kowalczewski, M. Liscidini, and L. C. Andreani, "Engineering Gaussian disorder at rough interfaces for light trapping in thin-film solar cells," Opt. Lett. **37**, 4868–4870 (2012).
11. D. Berman and J. S. Perkins, "The Kirchhoff approximation and first-order perturbation theory for rough surface scattering," J. Acoust. Soc. Am. **78**, 1045–1051 (1985).
12. J. A. Ogilvy and H. M. Merklinger, "Theory of wave scattering from random rough surfaces," J. Acoust. Soc. Am. **90**, 3382 (1991).
13. S. O. Rice, "Reflection of electromagnetic waves from slightly rough surfaces," Commun. Pure Appl. Math. **4**, 351–378 (1951).
14. N. Garcia and E. Stoll, "Monte Carlo calculation for electromagnetic-wave scattering from random rough surfaces," Phys. Rev. Lett. **52**, 1798–1801 (1984).
15. M. Nieto-Vesperinas and J. M. Soto-Crespo, "Monte Carlo simulations for scattering of electromagnetic waves from perfectly conductive random rough surfaces," Opt. Lett. **12**, 979–981 (1987).
16. I. Babuška, F. Nobile, and R. Tempone, "A stochastic collocation method for elliptic partial differential equations with random input data," SIAM Rev. **52**, 317–355 (2010).
17. D. Xiu and D. M. Tartakovsky, "Numerical methods for differential equations in random domains," SIAM J. Sci. Comput. **28**, 1167–1185 (2006).
18. C. Canuto and T. Kozubek, "A fictitious domain approach to the numerical solution of PDEs in stochastic domains," Numer. Math. **107**, 257–293 (2007).
19. J. E. Castrillón-Candás, F. Nobile, and R. F. Tempone, "Analytic regularity and collocation approximation for elliptic PDEs with random domain deformations," Comput. Math. Appl. **71**, 1173–1197 (2016).
20. X. Feng, J. Lin, and D. P. Nicholls, "An efficient Monte Carlo-transformed field expansion method for electromagnetic wave scattering by random rough surfaces," Commun. Comput. Phys. **23**, 685–705 (2018).
21. D. Gottlieb and S. Orszag, *Numerical Analysis of Spectral Methods: Theory and Applications* (Society for Industrial and Applied Mathematics, 1977).
22. J. Shen, T. Tang, and L.-L. Wang, *Spectral Methods* (Springer, 2011).
23. L. N. Trefethen, *Spectral Methods in MATLAB* (SIAM, 2000).
24. K. Ulmer, *Numerical Modeling of Electromagnetic Wave Scattering by Layered Random Surfaces* (Auburn University, 2020).
25. D. P. Nicholls, "Stable, high-order computation of impedance-impedance operators for three-dimensional layered medium simulations," Proc. R. Soc. London A **474**, 20170704 (2018).
26. R. Petit, *Electromagnetic Theory of Gratings* (Springer, 1980).
27. Y. He, D. P. Nicholls, and J. Shen, "An efficient and stable spectral method for electromagnetic scattering from a layered periodic structure," J. Comput. Phys. **231**, 3007–3022 (2012).
28. J. W. Strutt, "On the dynamical theory of gratings," Proc. R. Soc. London A **79**, 399–416 (1907).
29. G. J. Lord, C. E. Powell, and T. Shardlow, *An Introduction to Computational Stochastic PDEs* (Cambridge University, 2014).
30. A. Kirsch and P. Monk, "An analysis of the coupling of finite-element and Nyström methods in acoustic scattering," IMA J. Numer. Anal. **14**, 523–544 (1994).
31. A. Gillman, A. H. Barnett, and P. G. Martinsson, "A spectrally accurate direct solution technique for frequency-domain scattering problems with variable media," BIT Numer. Math. **55**, 141–170 (2014).
32. F. Collino, S. Ghanemi, and P. Joly, "Domain decomposition method for harmonic wave propagation: a general presentation," Comput. Method Appl. Math. **184**, 171–211 (2000).
33. A. Malcolm and D. P. Nicholls, "A field expansions method for scattering by periodic multilayered media," J. Acoust. Soc. Am. **129**, 1783–1793 (2011).
34. D. P. Nicholls, "On analyticity of linear waves scattered by a layered medium," J. Differ. Equations **263**, 5042–5089 (2017).
35. D. P. Nicholls, "Three-dimensional acoustic scattering by layered media: a novel surface formulation with operator expansions implementation," Proc. R. Soc. London A **468**, 731–758 (2011).
36. B. Després, "Méthodes de décomposition de domaine pour les problèmes de propagation d'ondes en régime harmonique. le théorème de borg pour l'équation de hill vectorielle," thesis (Université de Paris IX, 1991).
37. L. C. Evans, *Partial Differential Equations*, 2nd ed. (American Mathematical Society, 2010).
38. R. LeVeque, *Finite Difference Methods for Ordinary and Partial Differential Equations* (Society for Industrial and Applied Mathematics, 2007).
39. C. Johnson, *Numerical Solution of Partial Differential Equations by the Finite Element Method* (Cambridge University, 1987).
40. J. Hesthaven and T. Warburton, *Nodal Discontinuous Galerkin Methods* (Springer, 2008).
41. M. Deville, P. Fischer, and E. Mund, *High-order Methods for Incompressible Fluid Flow* (Cambridge University, 2002).

42. D. Colton and R. Kress, *Inverse Acoustic and Electromagnetic Scattering Theory* (Springer, 2013).
43. D. P. Nicholls and F. Reitich, "Shape deformations in rough surface scattering: improved algorithms," J. Opt. Soc. Am. A **21**, 606–621 (2004).
44. N. A. Phillips, "A coordinate system having some special advantages for numerical forecasting," J. Meteorol. **14**, 184–185 (1957).
45. J. Chandezon, G. Raoult, and D. Maystre, "A new theoretical method for diffraction gratings and its numerical application," J. Opt. **11**, 235–241 (1980).
46. O. Bruno and F. Reitich, "Numerical solution of diffraction problems: a method of variation of boundaries," J. Opt. Soc. Am. A **10**, 1168–1175 (1993).
47. R. A. Horn and C. R. Johnson, *Matrix Analysis*, 2nd ed. (Cambridge University, 2017).
48. R. Caflisch, "Monte Carlo and quasi-Monte Carlo methods," Acta Numer. **7**, 1–49 (1998).
49. G. Baker and P. Graves-Morris, *Padé Approximants* (Addison-Wesley, 1981).
50. J. Nuttall, "The convergence of Padé approximants of meromorphic functions," J. Math. Anal. Appl. **31**, 147–153 (1970).
51. J. Zinn-Justin, "Convergence of Padé approximants in the general case," Rocky Mt. J. Math. **4**, 325–330 (1974).